Eur. Phys. J. B **28**, 289–297 (2002)
DOI: 10.1140/epjb/e2002-00232-8

THE EUROPEAN PHYSICAL JOURNAL B

Molecular reorientation in pyrene hexafluoroarsenate salts

B. Pongs, T. Wokrina, S. Matejcek, C. Buschhaus, and E. Dormann[a]

Physikalisches Institut, Universität Karlsruhe, Wolfgang-Gaede-Str. 1, 76128 Karlsruhe, Germany

Received 22 March 2002
Published online 31 July 2002 –

Abstract. The quasi-one dimensional pyrene (PY) organic conductor $(PY)_7(PY)_4(AsF_6)_4{\cdot}4CH_2Cl_2$ shows parallel as well as 60° rotated PY radical cations in its stacks, but crystallizes in two different modifications I and II. One of the seven intra-stack pyrene molecules is susceptible to a reorientation by 60°, that is stable already at room temperature for modification II, but occurs at a hysteretic first order transition between 170 K and 240 K for modification I. Crystal structure, microwave conductivity and static magnetic susceptibility are typical for a quasi-one dimensional organic conductor with Peierls transition at T_P = 73 K (mod. I) or T_P = 105 K (mod. II). The pyrene radical packing is analysed by continuous wave and pulsed electron spin resonance measurements, using 9.45 GHz as well as 425 MHz as measuring frequency. Anisotropy of the conduction electron diffusion constant exceeds 1000 in the metallic phase.

PACS. 76.30.-v Electron paramagnetic resonance and relaxation – 61.66.Hq Organic compounds

1 Introduction

The revived interest in Luttinger liquids stimulated recent studies of quasi-one dimensional conductors like the Bechgaard salts as part of the search for systems manifesting charge-spin separation [1–3]. Charge and anion ordering transitions could be identified for organic conductors [4,5]. On the other hand, the influence of disorder on the Peierls transition was established theoretically [6,7]. For a systematic experimental investigation of the Peierls transition, arene radical cation salts are especially promising candidates.

Electrocrystallization, with anodic oxidation of the chosen aromatic flat hydrocarbon (arene) molecule, allows a rich choice of quasi-one dimensionally conducting radical cation salts to be grown [8,9]. Octahedral anions like the hexafluorides PF_6, AsF_6 or SbF_6 are frequently used counterions. Stoichiometry and conduction band filling can be influenced by variation of the solvent, counterion, starting concentration and growth temperature – to mention only some of the factors of influence – and most of all, by the choice of the arene. The preferred π-electron wave-function overlap pattern of the radical cation determines the molecular packing in the one-dimensional stack, this channel being surrounded in many cases not only by the counterions, but also by neutral arenes and solvent molecules. Overlap may be optimized by the inclination of the arene radicals with respect to the stacking direction. Temperature dependent volume changes are thus of importance, but for most arenes, the fundamental packing scheme is unique: parallel (0°) orientation for perylene, antiparallel (180°) for fluoranthene, or 90° for naphthalene [8–11]. Pyrene (PY) opens an unusual degree of freedom: 0°, 60° and 90° packing were all reported for different radical cation salts of this single arene [8,9].

In this contribution, we present the analysis of a 7:4 pyrene hexafluoroarsenate radical cation salt with the composition $(PY)_7(PY^\circ)_4(AsF_6)_4{\cdot}4CH_2Cl_2$ [12,13]. In its seven-pyrene stacking unit (Fig. 1), larger intermolecular separations with 0° packing and shorter separations with 60° packing are found [8]. We show that a partially reversible, hysteretic first order reorientation transition (at T_{rot}) occurs in one modification of this salt, named I, but not in the other, named II, if the temperature is varied and thus, *via* thermal contraction or expansion, the stack length. We identify the 60° reorientation jump of one of the seven pyrene molecules, combining continuous wave X-band electron spin resonance (ESR) and pulsed radiofrequency ESR. Because the reorientation seems to occur statistically for about 50%–70% of the respective sites in modification I of the salt, whereas it is already stabilized at room temperature for modification II, it is no surprise that due to this disorder the Peierls transition of modification I is manifested three dimensionally only at lower temperature T_P than that of modification II [12]. It is known from perylene radical cation salts, that disorder can suppress the three dimensional transition to the static, Peierls distorted phase even entirely [14]. In this contribution, we unravel the pyrene stacking and reorientation and its consequences on the electronic structure of this puzzling quasi-one dimensional conductor.

[a] e-mail: edo@piobelix.physik.uni-karlsruhe.de

Our paper is organized as follows: In Section 2, we summarize the applied experimental techniques and the most relevant results. Their discussion in Section 3 is structured into microwave conductivity (3.1), static magnetic susceptibility (3.2), X-band ESR analysis (3.3) and radio frequency pulsed ESR analysis (3.4), followed by the main conclusions in Section 4.

2 Experimental detail and results

Needle-like pyrene-hexafluoroarsenate crystals were grown from dichloromethane (CH_2Cl_2) solution using the well-known electrochemical techniques [8–11,15]. The appropriate description as $(PY)_7(PY^\circ)_4(AsF_6)_4{\cdot}4CH_2Cl_2$ was established by elemental analysis and crystal structure determination and is corroborated by g-tensor analysis.

At $T = 105\,K$, a triclinic primitive cell ($P\bar{1}$) was found. The unit cell can be doubled to retain a non-primitive, nearly orthorhombic cell, with parameters $a = 21.02(1)$ Å, $b = 14.43(1)$ Å and $c = 23.51(1)$ Å, $\alpha = 94.3(2)^\circ$, $\beta = 89.1(2)^\circ$ and $\gamma = 92.7(2)^\circ$ in which the c-axis coincides with the pyrene molecule stacking axis. Figure 1 shows that the pyrene radical stacks are surrounded by the counterions, solvent molecules and neutral pyrene molecules building the walls of the one dimensional channels. Seven pyrene molecules, stacked in c direction, build the repetition unit. Four of them define the 0° orientation, two are oriented (uniquely) at 60°, but one position exhibits 0°/60° disorder that is further studied below. The precise charge and spin distribution along the conducting stack is unknown. Thus, from the 7:4 stoichiometry, a 5/7 (or 0.714) filling of the one dimensional conduction band in an extended band scheme can be derived, but the detailed arrangement of band gaps is not known. We mention that a strict periodicity of a seven-pyrene stack with otherwise homogeneous charge distribution would result for the 7:4 stoichiometric salt in being a semiconductor with five filled and two empty subbands. However, microwave conductivity, measured by the cavity perturbation method [12,16], indicates non-activated conductivity parallel to the preferred direction at temperatures above T_P, and a rather large conductivity anisotropy. The different behavior of modification I and II is seen in Figure 2. The similarity of the T-dependences for $\sigma_\parallel$ and $\sigma_\perp$ for modification I, combined with the typically very large conductivity anisotropy of quasi-1D arene conductors, suggests that a small $\sigma_\parallel$ component is measured also for $\sigma_\perp$ in modification I. It is unclear, if this is caused by a pronounced mosaic structure of this radical cation salt or by the limited precision of the crystal orientation. It should be mentioned that most crystals studied by X-band ESR actually were twins or consisted of even more subunits with congruent stacking directions, however. The typical hysteresis of the structural transition for modification I at T_{rot} is also reflected by microwave conductivity (Fig. 2).

For measurement of the static magnetic susceptibility with a Quantum Design SQUID magnetometer, mod. I crystals had to be selected by ESR analysis. This is necessary because both modifications have different Peierls

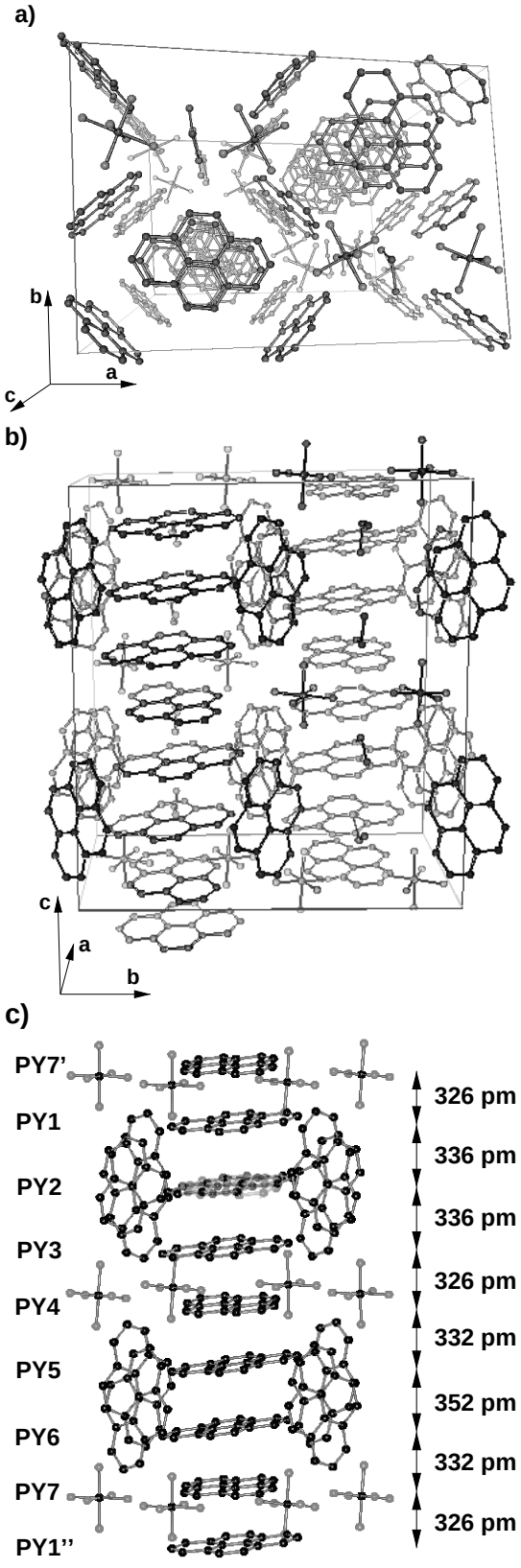

Fig. 1. Perspective view of pyrene stacks and surroundings in $(PY)_7(PY^\circ)_4(AsF_6)_4{\cdot}4CH_2Cl_2$, seen along (a) or perpendicular (b) to the stacking direction c. PY stacking separation, orientation and notation, as well as disorder of PY2 are shown in (c).

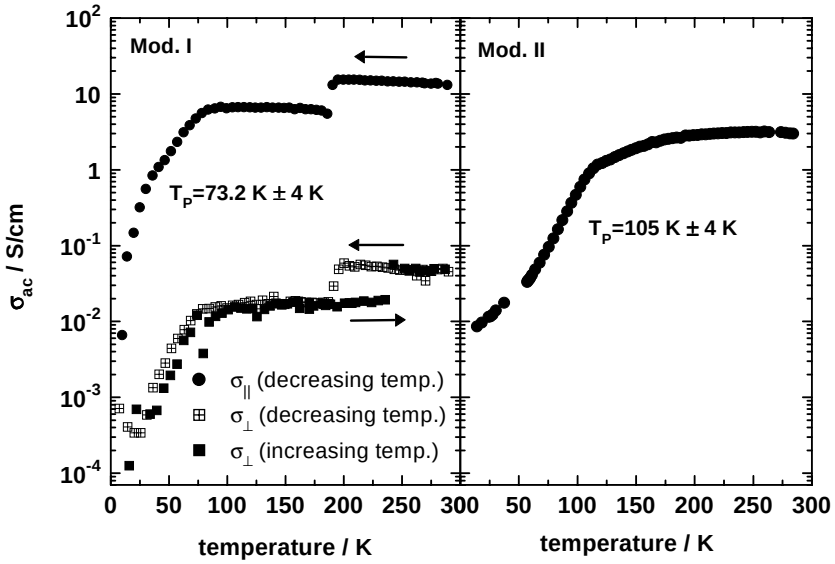

Fig. 2. Microwave conductivity of pyrene-hexafluoroarsenate crystals, modification I and II. (For mod. I, $\sigma_{\|}$ and $\sigma_{\perp}$ of the same crystal and typical hysteresis of $\sigma_{\perp}$ are shown.) Data recorded at 10.2 or 10.3 GHz during cooling of sample (except for $\sigma_{\perp}$).

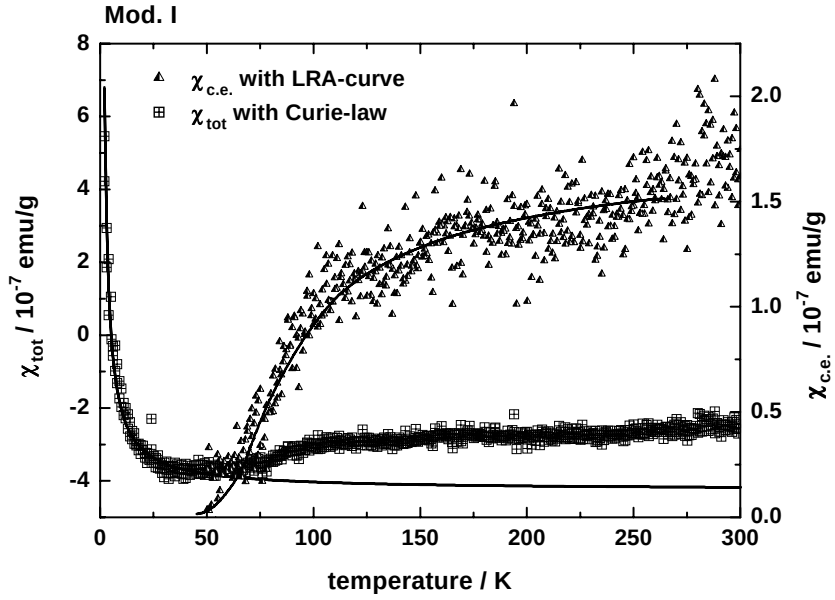

Fig. 3. Temperature dependence of magnetic susceptibility of many statistically oriented crystals of pyrene-hexafluoroarsenate salt, mod. I. Total susceptibility (left scale) and conduction electron contribution (right hand scale), measured for increasing temperature. For solid line fits see text.

transition temperatures T_P. Only mod. I has the additional structural transition at $T_{rot} > T_P$. Both modifications may be found in the same electrocrystallization run and can not be distinguished by their outer shape. The results for modification I are shown in Figure 3.

Due to the differing and partially even temperature dependent orientation of the stacked pyrene radicals, an inhomogeneous contribution of the g-anisotropy to the ESR line width (Fig. 4) in addition to ESR line splittings (Fig. 5) has to be struggled with in X-band ESR (recorded with a Bruker ESP 300 E spectrometer) of both modifications of PY-AsF_6 salt. Therefore the 2D technique COSY (correlation spectroscopy [17]) was applied with a Bruker ELEXSYS E-580 X-Band pulse spectrometer in order to examine the degree of interaction of the electron spins of different domains of the crystals (Fig. 6). The 90°-τ(var.)-180°-t(var.) spin echo sequence was adopted. The influence of the structural phase transitions of mod. I on electron spin transversal relaxation (T_2) was measured in function of temperature in the radiofrequency range (425 MHz) with a home-built set up [19], or a Tecmag APOLLO spectrometer as shown in Figure 7. The temperature dependence (Fig. 8) and anisotropy (Fig. 9) of the conduction electron spin diffusion constant were derived at 425 MHz by static magnetic field gradient spin echo decay analysis [18].

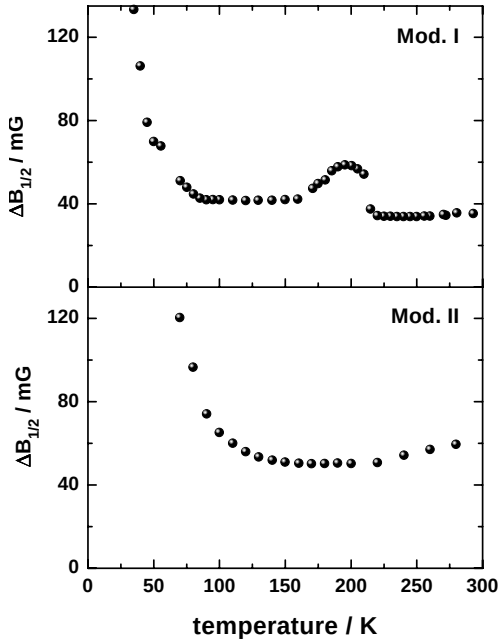

Fig. 4. Temperature dependence of ESR linewidth for pyrene-AsF_6 (mod. I and II) (9.45 GHz, measured for increasing temperature).

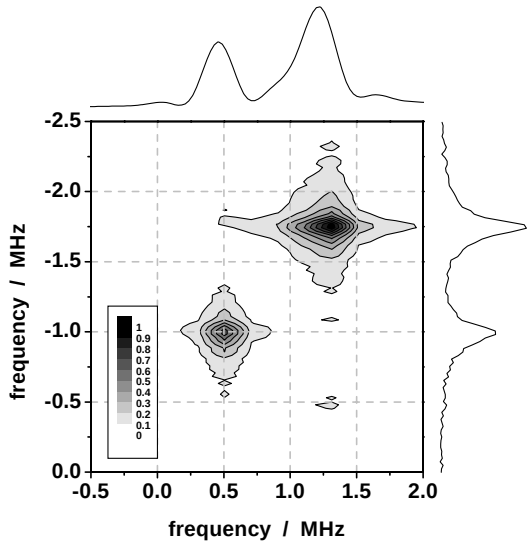

Fig. 6. 2D-COSY spectrum (correlation spectroscopy) of pyrene-AsF_6 (mod. I) at $T = 260$ K, $\nu = 9.5$ GHz, obtained by two-dimensional Fourier transformation from 90°-τ(var.)-180°-t(var.) spin echo sequence.

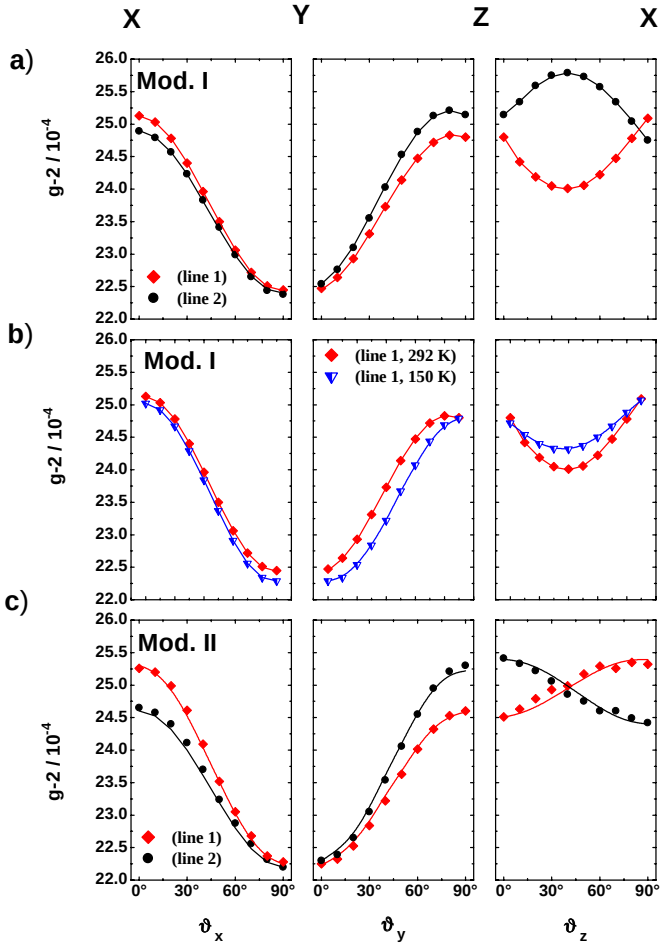

Fig. 5. Orientation dependence of the g-factor in laboratory frame (9.45 GHz) for pyrene-AsF_6 (mod. I (a) and II (c)) at 292 K and for one domain of mod. I at $T = 292$ K and 150 K (b). The Y-axis corresponds to the stacking axis (Fig. 1). Both lines of twinned crystals are analyzed in a) and c).

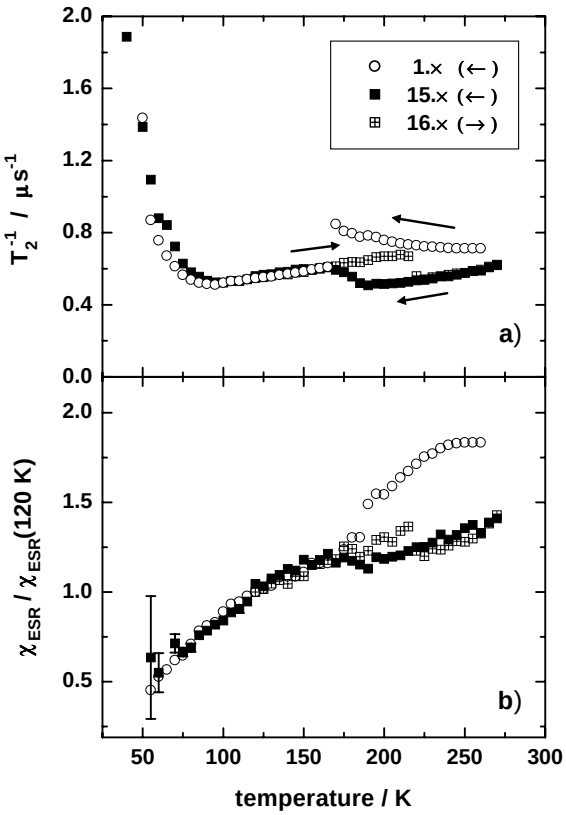

Fig. 7. (a) Temperature dependence of transversal relaxation rate T_2^{-1} in radiofrequency pulsed ESR of the pyrene-AsF_6 salt, mod. I. First and later (No. 15, solid squares) cooling run and subsequent heating run (16). (b) Temperature dependence of RF-ESR susceptibility for the same sample, normalized to 120 K.

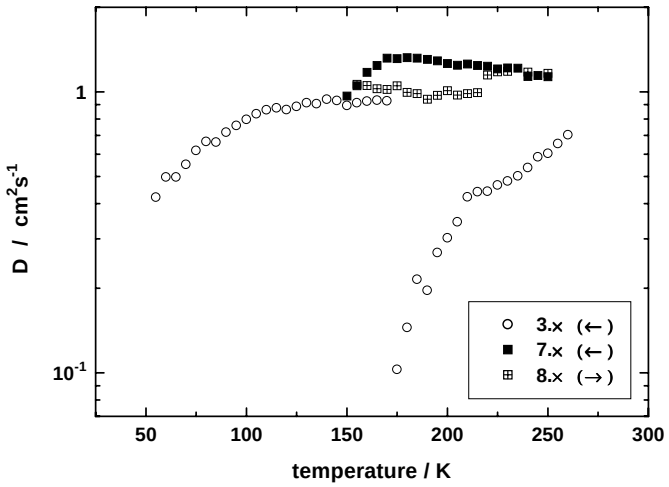

Fig. 8. Temperature dependence of the electron spin diffusion constant D parallel to stacking direction of pyrene-AsF_6 salt, mod. I derived by static magnetic field gradient spin echo ESR (425 MHz). The first cool-downs (*e.g.* 3.x) and later cooling-heating cycles have to be distinguished.

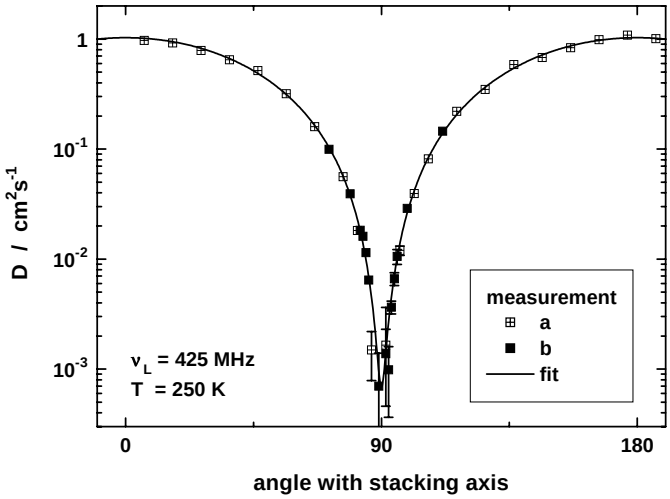

Fig. 9. Angular variation of the diffusion constant of a pyrene-AsF_6 (mod. I) salt (two measurements a and b) at $T = 250\,\mathrm{K} > T_{rot}$. The solid line shows the fit to equation 3 with $D_\parallel = 1.03\ \mathrm{cm^2/s}$ and $D_\perp = 6.8 \times 10^{-4}\,\mathrm{cm^2/s}$.

3 Discussion

3.1 Microwave conductivity

The temperature dependence of σ (Fig. 2) shows the behavior typically observed in arene salts with Peierls transition to a low temperature semiconducting CDW (charge density wave) ground state [20]. By analysis of $\mathrm{d}(\ln\sigma)/\mathrm{d}(1/T)$ in dependence of $1/T$, the Peierls transition temperatures T_P (Tab. 1) of both modifications of the 7:4 pyrene-AsF_6 salt are derived from the conductivity data. Modification I exhibits the more metal-like high-temperature variation of σ and the lower transition temperature T_P. Absolute values of the room temperature microwave conductivity parallel to the stacking direction are comparably small, however, indicative of the important role of defects and disorder in the macroscopic crystals. At T_{rot} (Tab. 1), reduction of the conductivity for lowering of T is observed. This first order transition shows considerable hysteresis, but the high-temperature absolute conductivity values suffer more from repeated temperature cycling than the low-temperature values, thus reducing the step-height for aged crystals of modification I. A large concentration of intra-stack defects, the disordered solvent molecules, the frozen-in disorder in the orientation (or reorientation) of one of the seven PY molecules in the stacking unit, subdividing the one-dimensional stack in low-temperature subunits of varied length, are evident reasons for the comparatively low absolute values of the microwave conductivity as well as of the Peierls-transition temperature T_P. They explain in addition the obvious smearing of the transition anomalies related with the Peierls transition (T_P).

Table 1. Parameters derived for $(PY)_7(PY^\circ)_4(AsF_6)_4 \cdot 4CH_2Cl_2$, modification I and II, by microwave conductivity and susceptibility measurement.

	Mod. I	Mod. II
T_P/K	73 ± 4	105 ± 4
T_{rot}/K	170-195/235-240	-
$\bar{x}^{\mathrm{def}}_{S=1/2}$/per f.u.	1.7×10^{-2}	
χ_{Pauli}/emu g^{-1}	1.62×10^{-7}	
T_{MF}/K	220	
$2\Delta_{\mathrm{eff}}$/K	360	

No well-defined activation of the conductivity in the low temperature range $T < T_P$ is observed under these conditions for the 7:4 pyrene salts. Tentatively, activation energies of $E_a = 14\,\mathrm{meV}$ (79–30 K, mod. I, $\sigma_\perp$) and $2\Delta = (6.8 \pm 0.8)\,\mathrm{meV}$ (48–20 K, mod. I), $2\Delta = (27.5 \pm 1.6)\,\mathrm{meV}$ (68–40 K, mod. II) were derived, useful as order of magnitude estimates.

The microwave conductivity measurements of the pyrene hexafluoroarsenate salts can also give a lower-limit of the anisotropy $\sigma_\parallel/\sigma_\perp > 100$, only, due to the needle shape of the not at all perfect crystals available.

3.2 Static magnetic susceptibility

The static magnetic susceptibility of mod. I crystals (Fig. 3) is separated into the contributions of molecular diamagnetism, Curie-like paramagnetic defects and conduction electrons according to

$$\chi_{tot} = \chi_{dia} + \frac{C}{T} + \chi_{c.e.}(T). \qquad (1)$$

The concentration x of localized $S = 1/2$ defects in the low temperature range (Tab. 1) is comparatively large in this pyrene radical cation salt, in agreement with the arguments given in Section 3.1.

The solid line fit to the $\chi_{c.e.}$ data of Figure 3 shows that for the average susceptibilty of many mod. I crystals,

the Lee-Rice-Anderson model [21] describes the temperature dependence, with the parameters of the limiting value of the Pauli susceptibility and the molecular field temperature T_{MF} given in Table 1, with high accuracy [12].

These parameters of the pyrene-AsF_6 salt (mod. I) can be compared with the earlier results for the fluoranthene salt $(FA)_2PF_6$ [22] and the perylene-AsF_6 salt $(PE)_2AsF_6 \cdot \frac{2}{3}$ THF, that is more clearly described as $(PE)_4(PE^{\circ})_2(AsF_6)_3 \cdot$ 2THF [23]. The limiting values of the conduction electron spin susceptibilities of all three quasi-1D conductors are quite similar, if expressed in units of 10^{-6} emu per one mole of in-stack arene radical cations, that is 66, 74 or 77 for FA, PE or PY, respectively. Thus the density of states in the metallic phase of all these arene salts is comparable. As far as the tendency to a Peierls distortion, T_{MF}, or the real 3D Peierls transition temperature, T_P, is concerned, there is a clear sequence from the simplest 2:1 FA-salt over the more complicated 4:3 PE salt to the most complicated 7:4 PY salt: T_{MF} decreases from 425 K over 253 K to 220 K, and T_P from 187 K over 102 K to 73 K. Thus also the ratio T_P/T_{MF}, *i.e.* 0.44, 0.40 or 0.33, decreases in this FA-PE-PY sequence, in support of the argument given above, that the Peierls-transition of pyrene-AsF_6 (mod. I) salts is depressed by disorder.

A barely temperature dependent effective energy gap of $2\Delta_{eff} \approx 31$ meV (360 K) would be sufficient to describe the variation of $\chi_{c.e.}$ for $T < T_P$ and $T_P < T < T_{rot}$ with the relation [24]

$$\frac{\chi_{c.e.}}{\chi_{\mathrm{Pauli}}} = 2 \int_{\Delta_{eff/k_BT}}^{\infty} \frac{x}{\sqrt{x^2 - \left(\frac{\Delta_{eff}}{k_BT}\right)^2}} \frac{\mathrm{e}^x}{(\mathrm{e}^x+1)^2} \mathrm{d}x. \quad (2)$$

The analysis of the average of many crystals prevents the decision, if this agreement is due to a distribution of Peierls transition temperatures or the absence of a really threedimensionally ordered Peierls distorted state in the mod. I pyrene-AsF_6 crystals. No drastic variation is observed for $\chi_{c.e.}$ at $T_{rot} \approx 240$ K. Thus X-band ESR is much more appropriate in order to unravel the structural variations at this transition, due to its sensibility to molecular reorientations *via* the g-tensor anisotropy, that reflects the pyrene radicals' orientation with respect to the external magnetic field [25].

3.3 X-band ESR analysis

Both modifications of the pyrene hexafluoroarsenate salt could easily be distinguished by the difference of their ESR linewidth at room temperature (Tab. 2). The smaller linewidth of modification I indicates, according to general experience, the more pronounced one-dimensional character of the electronic structure, in fair agreement with the lower Peierls-transition temperature of this modification. ESR analysis suffered from the fact that almost all crystals analyzed were at least twins, if not consistent of even more subunits. Their needle axis – used as "Y" axis of the laboratory frame in the g tensor analysis of Figure 5 – coincided, however, with the respective stacking direction and thus within 10° with the normal to the pyrene molecular plane (Fig. 1). This is the orientation with the smallest g-value of pyrene radicals (denoted g_c later on).

The linewidth of a separate ESR line in pyrene-AsF_6 varies with temperature by more than one order of magnitude, as is typical for arene radical cation salts [26–28]. Starting with a width of about 1 G for the Curie-like temperature dependent defect signals at temperatures below 10 K (1.3 G for mod. I, 0.7 G for mod. II), the line narrows, reaching a minimum close above the Peierls transition temperature, and increases then again with T, except for anomalies caused by unresolved line splittings close to T_{rot} for modification I (Fig. 4). Interference of homogeneous and inhomogeneous line broadening contributions makes a more detailed quantitative analysis untrustworthy, however.

The derivation of the individual stacks' g-tensors, collected in Table 2, presents the basis for the solid lines given for the resonance line orientation dependences in the laboratory frame in Figure 5, and forms a reliable basis for resolving the structural peculiarities of both pyrene-AsF_6 modifications. *A priori*, it was not clear, if the two ESR lines typically observed for a crystal belong to two neighbouring stacks with different orientation of the pyrene molecules or to two separate subunits (domains) of the crystal. By pulsed ESR correlation spectroscopy (COSY, [17]) (Fig. 6) the experimental proof was achieved that the two lines, followed in Figures 5a and c, belong to the two domains of twinned crystals, whose stacking axes coincide (g_c-orientation) but whose electron spins have negligible interaction. This conclusion is based on the absence of cross peaks in Figure 6. Primarily g_a and g_b of the twinned domains are interchanged. Both domains have sample dependent relative weights (see *e.g.* the 1D traces in Fig. 6).

For one domain, the changes of the g-anisotropy, caused by the structural phase transition of modification I, are shown in Figure 5b, with the calculated principle values g_a, g_b and g_c given in Table 2.

Since the g-tensor of individual pyrene radicals was derived recently for a 12:7 pyrene hexafluoroantimonate salt [25], the quantitative comparison of the respective values $g_x = 2.00274$, $g_y = 2.00235$ and $g_z = g_c = 2.00225$ ($\pm 2 \times 10^{-5}$) with the experimental values derived for mod. I and II of the Pyrene-AsF_6 salt reveals the crystallographic arrangement and rearrangement of the intrastack pyrene radicals as well as the electronic structure of these salts. First of all, the small value of g_c for both modifications of the hexafluoroarsenate salt studied here excludes the presence of spin density (and thus also charges) for the pyrene molecules oriented perpendicular to the stacks and forming the walls of the one-dimensional channels visible in Figure 1. Thus only the seven stacked pyrene molecules per repetition unit, with roughly uniform g_c-orientation, carry in the average the four free spins and charges corresponding to the 7:4 stoichiometry of the $(PY)_7^{4(+\bullet)}(PY^{\circ})_4(AsF_6^-)_4 \cdot 4CH_2Cl_2$ salt. The observed g_a and g_b values present the appropriate average over seven

Table 2. ESR parameters of both modifications of the pyrene-AsF_6 salt.

	mod. I ($T = 292\,\mathrm{K} > T_{rot}$)	mod. I ($T = 150\,\mathrm{K} < T_{rot}$)	mod. II ($T = 292\,\mathrm{K}$)
$\overline{\Delta B_{1/2}}$(290 K, 9.45 GHz)/mG	36		54
g_a	2.00259	2.00255	2.00254
g_b	2.00242	2.00243	2.00244
g_c	2.00224	2.00223	2.00223

$\Delta g : \pm 2 \times 10^{-5}$ absolute, $\pm 1 \times 10^{-6}$ relative error

g_x and g_y-values. According to crystal structure analysis, PY1, PY3, PY5, and PY6 are oriented parallel, and PY4 and PY7 rotated by 60° in the stack. Only PY2 is disorderd. Its degree of order and reorientation can be estimated from the g_a-g_b anisotropy which is largest for modification I and $T > T_{rot}$, but clearly smaller for $T < T_{rot}$ and modification II, respectively.

Thus g-tensor analysis indicates that the PY2 molecules are oriented predominantly in the 0°-orientation for the high temperature phase of modification I. According to the crystal structure analysis, a large PY-PY separation of about 3.5 Å is associated with parallel orientation of neighbouring PY molecules, and short PY-PY separation of about 3.3 Å with PY neighbours rotated by 60° (Fig. 1). An intermediate separation of the PY 2 molecule from the mutually parallel PY1 and PY3 sites points to the instability of its orientation. Thus, probably caused by reduced intra-stack separation during cooling down and accompanying lattice contraction [8], a part of the PY2 molecules rotates into the 60° orientation at T_{rot} of mod. I. According to g-tensor analysis this should happen for about 50–70% of the sites, increasing the disorder in the stack and for the PY2 site. Roughly the same degree of disorder is realized for modification II at room temperature already. We might surmise that a closer packing could be realized for modification II by a reduced concentration of the disordered solvent molecules.

3.4 Radiofrequency pulsed ESR analysis

One general advantage of RF-ESR analysis (425 MHz) is its insensitivity to the g-anisotropy and potential g-tensor distribution in multidomain or twinned crystals. Beyond that, pulsed (RF)-ESR, as applied here for pyrene-AsF_6 crystals, opens the possibility to discriminate clearly between different relaxation mechanisms (T_2, T_1) and the influence of electron spin diffusion ($D(\vartheta)$). Thus the temperature dependence of transversal relaxation (T_2) can be reliably derived. Figure 7a shows that the hysteretic behaviour around 200 K and the Peierls transition below 100 K are clearly reflected in $T_2(T)$. Two data sets originate from cooling run (15.x) and heating run (16.x) of a mod. I crystal. Very first cooling runs have to be distinguished from later cooling-heating cycles and will be discussed further below. *E.g.*, in the first runs, a wider hysteresis is observed (< 170 - > 225 K). RF-ESR susceptibility has been monitored at the same time, (Fig. 7b). It shows minor anomalies at the PY-reorientation phase transition, not surmounting 20 % variations, in agreement with the absence of pronounced anomalies for the temperature dependence of the average static magnetic susceptibility for many statistically oriented mod. I-crystals (Fig. 3). Thus for these later cycles, there is no indication for substantial variation of the conduction electron band width or of the interstack coupling at the PY-reorientation phase transition, T_{rot}, in contrast to their observed variation in $(PE)_2X{\cdot}2/3THF$ (X = PF_6, AsF_6; THF = tetrahydrofurane) at T_r [23,29]. Similar variation is observed for $T_1(T)$ as for $T_2(T)$. In the metallic phase above T_P, both relaxation rates increase with the number of cycles, except for typically the first one to three cycles (T_1, $T_2 \leq 3\,\mu$s, however). The general temperature dependence of T_1^{-1} and T_2^{-1} above and below the Peierls transition temperature follows the trends observed for Fluoranthene and Perylene radical cation salts [30,26], or for the linewidth of mod. II (Fig. 4): That means, both relaxation rates increase dramatically for decreasing temperature below the Peierls transition temperature T_P, because the decreasing number of conduction electrons is no more sufficient for exchange modulation of the radical defect electrons' hyperfine and conduction electron spin – defect spin mutual dipolar interaction. On the other hand, an almost linear increase of linewidth, $1/T_2$ and $1/T_1$ with T is typically observed above T_P. Since several mechanisms superimpose, quantitative separation of the relaxation contributions is generally difficult [18]. It is important to note that the anisotropy of the relaxation rates, derived in the metallic range of mod. I crystals in the RF range, is above the error limit, but not above 10 % of the respective temperature dependent value.

The dependence of the T_2^{-1} relaxation rate on the number of cooling and heating cycles accords with expectation for the case that the concentration of localized defects increases with cycle number. For radiation induced defects in Fluoranthene radical cation salts, the ESR linewidth was reported to decrease at first with increasing defect concentration x up to about $x \approx 1\,\%$ per $(FA)_2$ and to increase thereafter (up to much larger values) for larger defect concentration [31]. Thus x-dependence and cycle number dependence seem to be related.

In the first cooling run of a mod. I crystal, a behaviour of T_2^{-1}, χ_{ESR} and $D_{\|}$ differing from later cycles was generally observed in the RF-ESR analysis. The relaxation rate, T_2^{-1}, increases with decreasing T on approach to

T_{rot}, jumping to a smaller value at the transition (Fig. 7a). This seems to reflect the PY-librational slowing down and rotational disorder, that has a dramatic influence also on the conduction electron spin diffusion constant parallel to the stacking direction, $D_{\|}$, shown in Figure 8. At the third approach to T_{rot} during cool-down the diffusion constant decreases by almost one order of magnitude, whereas hysteretic variation by only about 20 % is registered for typical later cycles. Similar deviation of the first cycles is observed for the ESR susceptibility (Fig. 7b), that decreases with T approaching T_{rot} much more than in the subsequent cycles. We remind that comparable cycling consequences were seen for the microwave conductivity (Sect. 3.1), revealing an influence of the early packing changes on the electronic structure of pyrene-AsF_6 (mod. I).

The temperature dependence of absolute value and anisotropy of the conduction electron spin diffusion constant is reliably derived by static magnetic field gradient spin-echo RF-ESR [18]. The variation of $D(\vartheta)$ with the angle ϑ with respect to the stacking axis can accurately be described by

$$D(\vartheta) = D_{\|}\cos^2\vartheta + D_{\perp}\sin^2\vartheta. \quad (3)$$

For the same crystal analyzed in Figures 7 and 8, the variation shown in Figure 9 yields $D_{\|} = (1.03 \pm 0.01)$ cm^2/s and $D_{\perp} = (6.8 \pm 0.7) \times 10^{-4}$ cm^2/s, thus an anisotropy of $D_{\|}/D_{\perp} \approx 1500$ at $T = 250$ K ($> T_{rot}$). Due to the ease of systematic variation of ϑ the anisotropy is thus larger and more reliably accessed here than in the microwave conductivity measurement for two fixed orientations (Fig. 2). These results prove that pyrene-AsF_6 crystals exhibit pronounced anisotropy of their transport properties inspite of the disorder and substantial defect concentration derived above.

4 Conclusions

The radical cation salt pyrene hexafluoroarsenate is a quasi-one dimensional conductor with chemically an 11:4 (2.75:1) composition, but electronically a 7:4 stoichiometry. Seven pyrene radicals belong to one unit of the 1D stack (Fig. 1) and are surrounded by neutral pyrene molecules according to a sum formula $(PY)_7^{4(+\bullet)}(PY^{\circ})_4(AsF_6^-)_4{\cdot}4CH_2Cl_2$. Provided that all pyrene radicals have equal charge and uniform separation, a 5/7 filling of the conduction band is predicted for a 7:4 stoichiometry in the extended band scheme. If the only additional periodicity is a strict seven-pyrene stack length, the large Brillouin zone is broken down in parts of one seventh, and the respective seven subbands are filled up to the top of the fifth one. Microwave conductivity indicates the absence of a pronounced gap, however (Fig. 2), and the X-ray analysis proves that the pyrene radical cations are not uniformly packed. Furthermore, due to the disordered orientation of the PY2 molecule (Fig. 1) the length of the individual PY-stacking sequence deviates from the unit cell length of seven PY spacings. According to X-ray and ESR-g tensor analysis, in the high-temperature phase of modification I, comparatively high degree of order is preserved in a $-0°-0°-0°-60°-0°-0°-60°$-packing of the stacked pyrenes. This sequence is partially (*i.e.* 50–70 %) replaced by a $-0°-60°-0°-60°-0°-0°-60°$-sequence for the low-temperature phase of modification I, or, generally, in the modification II. Thus these radical cation salts exhibit substantial disorder, which explains that the Peierls transition temperatures are low and the transitions are not accompanied by very pronounced anomalies in magnetic susceptibility or microwave conductivity. Considerable hysteresis is found for the structural phase transition (T_{rot}) that results in the 0° to 60° degree reorientation of the PY2-sites of modification I. Yet for both modifications, and on both sides of these PY2-sites, a $-0°-60°-0°$-sequence is preserved. Inspection of Figure 1 reveals that these stable molecules might well be subject to a stronger influence of the neighbouring counter ions or the polar CH_2Cl_2 solvent molecules, respectively, than the PY2-sites. The latters primarily are caged by the four neutral pyrene molecules of the channel wall, and thus especially sensitive to the temperature dependent overlap strength along the conduction stack. Less freedom for high-temperature rotation of the PY2-molecules is left in mod. II-crystals than in mod. I-crystals. We argue that this difference may be correlated with the actual solvent content of the individual crystal.

More generally, the above analysis of the pyrene hexafluoroarsenate salt presents another example [25] for the relevant role of librational degrees of freedom of the stacked arene radical cations in such highly anisotropic, really organic conductors classified as CDW-Peierls systems. We remember: pyrene is $C_{16}H_{10}$, and the conduction electrons analyzed reside in extended π electron molecular orbitals, whose electron spin resonance g-tensor principal values are close to the free electron g-factor, but reflect nevertheless the molecular structure and orientation rather reliably. Most remarkably, the weak spin orbit coupling at light atoms and for one-dimensionally restricted motion guarantees long relaxation times for the coupled system of the defect spins and the conduction electron spins opening access to the numerous measuring techniques of continuous wave and pulsed electron spin resonance, some of which were exploited in this report.

We thank I. Odenwald for growing the crystals, and M.T. Kelemen for SQUID magnetometry. This work was financially supported by the Deutsche Forschungsgemeinschaft within Sonderforschungsbereich 195 (Universität Karlsruhe).

References

1. J. Voit, Physica C **282-287**, 1747 (1997)
2. A. Georges, T. Giamarchi, N. Sandler, Phys. Rev. B **61**, 16393 (2000)
3. F. Zwick, M. Grioni, G. Margaritondo, V. Vescoli, L. Degiorgi, B. Alavi, G. Grüner, Solid State Commun. **113**, 179 (2000)
4. D. Jérome, *Organic conductors*, edited by J.P. Farge (Marcel Dekker, New York, 1994), p. 405

5. F. Nad, P. Monceau, C. Carcel, J.M. Fabre, Phys. Rev. B **62**, 1753 (2000); J. Phys. Cond. Matt. **13**, L 717 (2001)
6. L. Bartosch, Ann. Phys. (Leipzig) **10**, 799 (2001)
7. I. Baldea, H. Köppel, L.S. Cederbaum, Phys. Rev. B **55**, 1481 (1997)
8. V. Enkelmann, K. Göckelmann, Ber. Bunsenges. Phys. Chem. **91**, 950 (1987)
9. V. Enkelmann, Adv. Chemistry Ser. **217**, 177 (1988)
10. H. Endres, H.J. Keller, B. Müller, D. Schweitzer, Acta Crystallogr. C **41**, 607 (1985)
11. H.P. Fritz, H. Gebauer, P. Friedrich, P. Ecker, R. Artes, K. Schubert, Z. Naturforsch. b **33**, 498 (1978)
12. B. Pongs, S. Matejcek, M.T. Kelemen, C. Buschhaus, E. Dormann, Synth. Metals **120**, 839 (2001)
13. V. Enkelmann, Habilitationsschrift, Universität Freiburg (1983), unpublished
14. C. Buschhaus, R. Desquiotz, K. Eichhorn, M. Hofmann, K. Hümmer, V. Illich, M.T. Kelemen, S. Tarragona Auga, T. Wokrina, A. Zitsch, E. Dormann, Eur. Phys. J. B **8**, 57 (1999)
15. B. Pongs, Ph.D. Thesis, Universität Karlsruhe (Shaker, Aachen 2001)
16. G. Schaumburg, H.W. Helberg, J. Phys. III France **4**, 917 (1994)
17. S. Braun, H.-O. Kalinowski, S. Berger, 150 and more basic NMR experiments (Wiley-VCH, 1998)
18. T. Wokrina, E. Dormann, N. Kaplan, Phys. Rev. B **54**, 10492 (1996)
19. P. Rösch, M.T. Kelemen, T. Wokrina, E. Dormann, Meas. Sci. Technol. **11**, 1610 (2000)
20. W. Brütting, W. Rieß, M. Schwoerer, Ann. Physik **1**, 409 (1992)
21. P.A. Lee, T.M. Rice, P.W. Anderson, Phys. Rev. Lett. **31**, 462 (1973)
22. U. Köbler, J. Gmeiner, E. Dormann, J. Magn. Magn. Mater. **69**, 189 (1987)
23. R. Desquiotz, M. Hofmann, E. Dormann, Eur. Phys. J. B **16**, 403 (2000)
24. D.C. Johnston, Phys. Rev. Lett. **52**, 2049 (1984)
25. B. Pongs, E. Dormann, Phys. Rev. B **65**, 144451 (2002)
26. A. Wolter, U. Fasol, R. Jäppelt, E. Dormann, Phys. Rev. B **54**, 12272 (1996)
27. E. Müller, J.H.v. Schütz, H.C. Wolf, J. Phys. Colloq. France **44**, C3-1401 (1983)
28. E. Müller, J.H.v. Schütz, H.C. Wolf, Mol. Cryst. Liq. Cryst. **93**, 407 (1983)
29. C. Buschhaus, R. Moret, S. Ravy, E. Dormann, Synth. Metals **108**, 179 (2000)
30. G. Sachs, W. Stöcklein, B. Bail, E. Dormann, M. Schwoerer, Chem. Phys. Lett. **89**, 179 (1982)
31. J.M. Delrieu, M. Beguin, M. Sanquer, Synth. Metals **19**, 361 (1987)